Time-resolved axial-view of the dielectric breakdown under tight focusing in glass

Yoshio Hayasaki,[1,*] **Keisuke Iwata,**[1] **Satoshi Hasegawa,**[1]
Akihiro Takita,[1] **and Saulius Juodkazis**[2,3]

[1]*Center for Optical Research and Education (CORE), Utsunomiya University, 7-1-2 Yoto, Utsunomiya 321-8585, Japan*
[2]*Centre for Micro-Photonics, Faculty of Engineering and Industrial Sciences, Swinburne University of Technology, Hawthorn, VIC 3122, Australia*
[3]*Melbourne Centre for Nanofabrication, 151 Wellington Road, Clayton, VIC 3168, Australia*
[*]*hayasaki@opt.utsunomiya-u.ac.jp*

Abstract: We present time-resolved studies of the dielectric breakdown using tightly focused femtosecond (fs) laser pulses in glass. Axial evolution of the breakdown and material modifications have been retrieved over the time span from 0 to 1 ns with a 50 fs resolution and ~ 1 μm spatial resolution using interferometric pump-probe technique. It is shown that even at pulse power slightly above critical $P_{cr} \simeq 1$ MW/pulse, the filamentation was limited at tight focusing and the central focal region with resolidified glass was localised axially within ~ 10 μm; it can be used for the waveguide recording. Mechanisms of light-matter interaction at tight focusing and application potential are discussed. The electron-ion scattering time, $\tau_{e-i} \simeq 1.1$ fs, for the glass at electron concentration $n_e \simeq (4-5)\times 10^{20}$ cm^{-3} was determined within Drude approximation.

OCIS codes: (140.3390) Laser material processing; (350.3850) Materials processing; (160.1245) Artificially engineered materials.

References and links

1. Y. Hayasaki, M. Isaka, A. Takita, and S. Juodkazis, "Time-resolved interferometry of femtosecond-laserinduced processes under tight focusing and close-to optical breakdown inside borosilicate glass," Opt. Express **19**, 5725–5734 (2011).
2. Q. Sun, H. Jiang, Y. Liu, Z. Wu, H. Yang, and Q. Gong, "Measurement of the collision time of dense electronic plasma induced by a femtosecond laser in fussed silica," Opt. Lett. **30**, 320–322 (2005).
3. A. Mermillod-Blondin, C. Mauclair, J. Bonse, R. Stoian, E. Audouard, A. Rosenfeld, and I. V. Hertel, "Time-resolved imaging of laser-induced refractive index changes in transparent media," Rev. Sci. Instrum. **82**, 033703 (2011).
4. M. Sakakura, M. Terazima, Y. Shimotsuma, K. Miura, and K. Hirao, "Thermal and shock induced modification inside a silica glass by focused femtosecond laser pulse," J. Appl. Phys. **109**, 023503 (2011).
5. S. Juodkazis, S. Kohara, Y. Ohishi, N. Hirao, A. Vailionis, V. Mizeikis, A. Saito, and A. Rode, "Structural changes in femtosecond laser modified regions inside fused silica," J. Opt. **12**, 124007 (2010).
6. A. Vailionis, E. G. Gamaly, V. Mizeikis, W. Yang, A. Rode, and S. Juodkazis, "Evidence of super-dense aluminum synthesized by ultra-fast micro-explosion," Nat. Commun. **2**, 445 (2011).
7. S. Nolte, M. Will, J. Burghoff, and A. Tünnermann, "Femtosecond waveguide writing: a new avenue to three-dimensional integrated optics," Appl. Phys. A **77**, 109–111 (2003).
8. G. Cerullo, R. Osellame, S. Taccheo, M. Marangoni, D. Polli, R. Ramponi, P. Laporta, and S. D. Silvestri, "Femtosecond micromachining of symmetric waveguides at 1.5μm by astigmatic beam focusing," Opt. Lett. **27**, 1938–1940 (2002).

#153140 - $15.00 USD Received 19 Aug 2011; revised 3 Oct 2011; accepted 9 Oct 2011; published 2 Nov 2011

9. M. Ams, G. D. Marshall, P. Dekker, J. A. Piper, and M. J. Withford, "Ultrafast laser written active devices," Laser Photon. Rev. **3**, 535–544 (2009).
10. Y. Bellouard, M. Dugan, A. A. Said, and P. Bado, "Thermal conductivity contrast measurement of fused silica exposed to low-energy femtosecond laser pulses," Appl. Phys. Lett. **89**, 161911 (2006).
11. A. Benayas, D. Jaque, B. McMillen, and K. P. Chen, "High repetition rate UV ultrafast laser inscription of buried channel waveguides in sapphire: Fabrication and fluorescence imaging via ruby R lines," Opt. Express **17**, 10076–10081 (2009).
12. G. Cheng, K. Mishchik, C. Mauclair, E. Audouard, and R. Stoian, "Ultrafast laser photoinscription of polarization sensitive devices in bulk silica glass," Opt. Express **17**, 9515–9525 (2009).
13. S. M. Eaton, H. Zhang, M. L. Ng, J. Z. Li, W. J. Chen, S. Ho, and P. R. Herman, "Transition from thermal diffusion to heat accumulation in high repetition rate femtosecond laser writing of buried optical waveguides," Opt. Express **16**, 9443–9458 (2008).
14. W. Gawelda, D. Puerto, J. Siegel, A. Ferrer, A. R. de la Cruz, H. Fernandez, and J. Solis, "Ultrafast imaging of transient electronic plasmas produced in conditions of femtosecond waveguide writing in dielectrics," Appl. Phys. Lett. **93**, 121109 (2008).
15. L. Bressel, D. de Ligny, C. Sonneville, V. Martinez-Andrieux, V. Mizeikis, R. Buividas, and S. Juodkazis, "Femtosecond laser induced density changes in GeO_2 and SiO_2 glasses: fictive temperature effect," Opt. Mater. Express **1**, 605–613 (2011).
16. K. M. Davis, K. Miura, N. Sugimoto, and K. Hirao, "Writing waveguides in glass with a femtosecond laser," Opt. Lett. **21**, 1729–1731 (1996).
17. C. E. Bell and J. A. Landt, "Laser-induced high-pressure shock waves in water," Appl. Phys. Lett. **10**, 46–48 (1967).
18. A. Vogel, S. Busch, and U. Parlitz, "Shock wave emission and cavitation bubble generation by picosecond and nanosecond optical breakdown in water," J. Acoust. Soc. Am. **100**, 148–165 (1996).
19. A. B. Schaffer, N. Nishimura, E. N. Glezer, A. M.-T. Kim, and E. Mazur, "Dynamics of femtosecond laser-induced breakdown in water from femtoseconds to microseconds," Opt. Express **10**, 196–203 (2002).
20. E. Abraham, K. Minoshima, and H. Matsumoto, "Femtosecond laser-induced breakdown in water: time-resolved shadow imaging and two-color interferometric imaging," Opt. Commun. **176**, 441–452 (2000).
21. X. Zeng, X. Mao, S. S. Mao, A.-B. Wen, R. Greif, and E. Russo, "Laser-induced shockwave propagation from ablation in a cavity," Appl. Phys. Lett. **88**, 061502 (2006).
22. V. V. Temnov, K. S.-Tinten, P. Zhou, and D. von der Linde, "Ultrafast imaging interferometry at femtosecond-laser-excited surfaces," J. Opt. Soc. Am. B **23**, 1954–1964 (2006).
23. A.Takita and Y. Hayasaki, "Interference measurement of superposition of laser-induced shock waves in water," Jpn. J. Appl. Phys. **48**, 09LD04 (2009).
24. T. Balčiunas, A. Melninkaitis, G. Tamosauskas, and V. Sirutkaitis, "Time-resolved off-axis digital holography for characterization of ultrafast phenomena in water," Opt. Lett. **33**, 58–60 (2008).
25. A. Marcinkevicius, V. Mizeikis, S. Juodkazis, S. Matsuo, and H. Misawa, "Effect of refractive index-mismatch on laser microfabrication in silica glass," Appl. Phys. A **76**, 257–260 (2003).
26. E. Gaižauskas, E. Vanagas, V. Jarutis, S. Juodkazis, V. Mizeikis, and H. Misawa, "Discrete damage traces from filamentation of Bessel-Gauss pulses," Opt. Lett. **31**, 80–82 (2006).
27. E. E. Gamaly, S. Juodkazis, K. Nishimura, H. Misawa, B. Luther-Davies, L. Hallo, P. Nicolai, and V. Tikhonchuk, "Laser-matter interaction in a bulk of a transparent solid: confined micro-explosion and void formation," Phys. Rev. B **73**, 214101 (2006).
28. L. Sudrie L, M. Franco, B. Prade, and A. Mysyrowicz, "Study of damage in fused silica induced by ultra-short IR laser pulses," Opt. Commun. **191**, 333–339 (2001).
29. S. Juodkazis, H. Misawa, O. A. Louchev, and K. Kitamura, "Femtosecond laser ablation of chalcogenide glass: explosive formation of nano-fibers against thermo-capillary growth of micro-spheres," Nanotechnology **17**, 4802–4805 (2006).
30. S. Juodkazis, K. Nishimura, S. Tanaka, H. Misawa, E. E. Gamaly, B. Luther-Davies, L. Hallo, P. Nicolai, and V. Tikhonchuk, "Laser-induced microexplosion confined in the bulk of a sapphire crystal: Evidence of multi-megabar pressures," Phys. Rev. Lett. **96**, 166101 (2006).
31. S. Juodkazis, H. Misawa, T. Hashimoto, E. Gamaly, and B. Luther-Davies, "Laser-induced micro-explosion confined in a bulk of silica: formation of nano-void," Appl. Phys. Lett. **88**, 201909 (2006).
32. T. Hashimoto, S. Juodkazis, and H. Misawa, "Void formation in glass," New J. Phys. **9**, 253 (2007).
33. S. Juodkazis, N. Murazawa, H. Wakatsuki, and H. Misawa, "Laser irradiation induced disintegration of a bubble in a glass melt," Appl. Phys. A **87**, 41–45 (2007).
34. M. Malinauskas, A. Žukauskas, G. Bičkauskaitė, R. Gadonas, and S. Juodkazis, "Mechanisms of three-dimensional structuring of photo-polymers by tightly focussed femtosecond laser pulses," Opt. Express **18**, 10209–10221 (2010).
35. M. Malinauskas, P. Danilevičius, and S. Juodkazis, "Three-dimensional micro-/nano-structuring via direct write polymerization with picosecond laser pulses," Opt. Express **19**, 5602–5610 (2011).
36. E. Gamaly, S. Juodkazis, V. Mizeikis, H. Misawa, A. Rode, and W. Krolokowski, "Modification of refractive

#153140 - $15.00 USD Received 19 Aug 2011; revised 3 Oct 2011; accepted 9 Oct 2011; published 2 Nov 2011

index by a single fs-pulse confined inside a bulk of a photo-refractive crystal," Phys. Rev. B **81**, 054113 (2010).
37. S. Juodkazis, V. Mizeikis, and H. Misawa, "Three-dimensional microfabrication of materials by femtosecond lasers for photonics applications," J. Appl. Phys. **106**, 051101 (2009).
38. L. Hallo, C. Mézel, A. Bourgeade, D. Hébert, E. G. Gamaly, and S. Juodkazis, "Laser-matter interaction in transparent materials: confined micro-explosion and jet formation," in *Extreme Photonics and Applications*, T. J. Hall, S. V. Gaponenko, and S. A. Paredes, eds. (Springer Netherlands, 2009), pp. 121–146.
39. Y. Hayasaki, T. Sugimoto, A. Takita, and N. Nishida, "Variable holographic femtosecond laser processing by use of spatial light modulator," Appl. Phys. Lett. **87**, 031101 (2005).
40. L. Bressel, D. de Ligny, C. Sonneville, V. Martinez-Andrieux, and S. Juodkazis, "Laser-induced structural changes in pure GeO_2 glasses," J. Non-Crystal. Sol. **357**, 2637–2640 (2011).
41. K. Hatanaka, T. Ida, H. Ono, S.-I. Matsushima, H. Fukumura, S. Juodkazis, and H. Misawa, "Chirp effect in hard X-ray generation from liquid target when irradiated by femtosecond pulses," Opt. Express **16**, 12650–12657 (2008).
42. D. M. Krol, "Femtosecond laser modification of glass," J. Non-Cryst. Solids **354**, 416–424 (2009).
43. S. K. Sundaram and E. Mazur, "Inducing and probing non-thermal transitions in semiconductors using femtosecond laser pulses," Nat. Mater. **1**, 217–224 (2002).
44. C. W. Carr, J. D. Bude, and P. DeMange, "Laser-supported solid-state absorption fronts in silica," Phys. Rev. B **82**, 184304 (2010).
45. S. G. Demos, M. Staggs, and M. R. Kozlowski, "Investigation of processes leading to damage growth in optical materials for large-aperture lasers," Appl. Opt. **41**, 3628–3633 (2002).
46. S. D. McGrane, A. Grieco, K. J. Ramos, D. E. Hooks, and D. S. Moore, "Femtosecond micromachining of internal voids in high explosive crystals for studies of hot spot initiation," J. Appl. Phys. **105**, 073505 (2009).

1. Introduction

Recently, we have demonstrated development of an interferometric pump-probe time-resolved imaging technique capable to characterize modifications in glass induced by fs-laser pulses [1] in the *lateral* cross section of the pulse propagation at the conditions close to the dielectric breakdown and with spatial resolution of ~ 1 μm. Important and unseen *axial* evolution of the light-matter interaction and breakdown has not been observed so far at the focusing under oil-immersion conditions, i.e., when numerical aperture of the objective lens was $NA > 1$. Earlier studies of the filamentation and breakdown were carried out at less tight focusing for the side-view imaging [2–4] with length of single filaments in sub-millimeter range. The side-view of the laser pulse interaction in glasses and crystals has to be achieved with resolution of several micrometers in space and tens-of-fs in time in order to fully characterize sequence of the processes which initiate a long relaxation towards the final state when different outcomes are expected: permanent void formation, densification at the focus, or synthesis of new nano-materials via elemental separation in plasma [5, 6]. The high resolution space-time imaging is essential for characterization of the breakdown and filamentation at tight focussing and will guide development of the direct laser writing of waveguides [7–14] and new compositions of glasses where engineering of their thermal response [15] at the focus would lead to self-occurring densification of the waveguiding region as observed in silica [16]. The established interferometric and shadowgraphy methods [17–24] have to be adopted for investigation of light-matter (liquid and solid) interaction with the high spatial and temporal resolutions simultaneously.

Here we demonstrate time-resolved transient of the dielectric breakdown at tight focusing and at pulse power slightly above self-focusing threshold. The pump-probe method was applied to resolve amplitude and phase changes of interferograms obtained by a Michelson interferometer. The axial length of the modified region was only ~ 9 μm and was only 4-5 times longer than the geometrical focal extension of the focus. The electron - ion scattering time was obtained using Drude model.

2. Experimental

The pump-probe (800 nm - 400 nm) fs-laser setup for single-pulse measurements was described in our recent work [1], where it was used to characterize the lateral view at the pre-

#153140 - $15.00 USD Received 19 Aug 2011; revised 3 Oct 2011; accepted 9 Oct 2011; published 2 Nov 2011

breakdown conditions. Differently from that geometry, here, we implement the axial view approach schematically shown in Fig. 1(a).

The interferometric detection part was the same as in the previous work and the actual setup is shown in Fig. 1(b). The fast Fourier transform (FFT) and filtering procedures were the same as used earlier [1]. The resolution limit of the optical imaging part was 0.58 μm for the $\lambda_{pr} =$ 400 nm using an objective lens of numerical aperture $NA = 0.42$. The resolution limit of the image processing was $r_{ip} = 1/h = 0.94$ μm defined by the cutoff frequency h of the Hann window $W(\nu)$ described by:

$$\begin{aligned} W(\nu) &= \frac{1}{2}\left[1+\cos\left(\frac{\pi|\nu-\nu_c|}{h}\right)\right] \quad \text{if } |\nu-\nu_c| \le h \\ &= 0 \qquad\qquad\qquad\qquad\qquad\qquad\quad \text{otherwise} \end{aligned} \tag{1}$$

where ν_c is the spatial frequency of interference fringes. Therefore, the resolution limit imposed by the image processing was slightly larger than the ideal diffraction-limited diameter of the pump pulse. Numerically retrieved amplitude and phase images via Fourier routine were analyzed. The phase maps of the axial view of the focal region are obtained with the highest spatial resolution so far. The focal spot was located at approximately 10 μm below surface inside a superwhite crown glass (B270, Schott). The amplitude data are also presented side by side with the phase, however, interpretation of the amplitude, which is proportional to the absorption coefficient, has ambiguity due to strong changes of absorption in solid and molten phases [22]. Hence, we discuss amplitude maps only qualitatively.

Location of the geometrical focus has been determined at low pulse energies when small positive phase changes were induced and spherical aberration was negligible [25] since the immersion oil is matching the refractive index of crown glass, $n_0 = 1.517$. The waist at the focus is estimated as $\omega = 0.61\lambda/NA \simeq 0.39$ μm which is a radius of the Airy disk pattern. The depth of focus - the double Rayleigh length $2z_R = 2\frac{\pi\omega^2}{\lambda}n_0 \simeq 1.8$ μm (at FWHM), where $\lambda = 0.8$ μm is the central wavelength of the laser pump pulse in air.

Pump pulse energy, E_p, is given at the focus; the transmission of objective lens was directly measured. The threshold of self-focusing in glass is ~ 1.8 MW [26] and is lower than in pure silica by a factor of two. The side imaging was carried out with 400 nm probe with $NA =$ 0.42 objective lens. The smallest recognizable features were on the order of ~ 1 μm and were slightly larger than the ideal diffraction limited focus of the pump pulse. Experiments were carried out at pump pulse energies $E_p = 10 - 1000$ nJ to explore the breakdown and formation

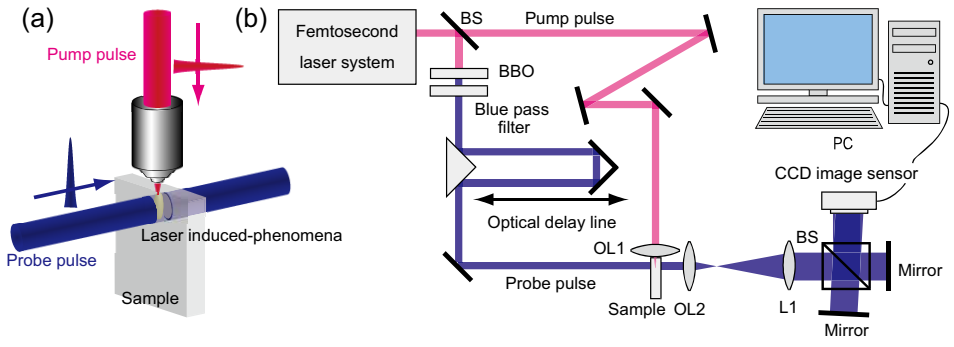

Fig. 1. Principle (a) and realization (b) of interferometric pump-probe side-imaging; an actual interferogram is shown on the PC screen.

#153140 - $15.00 USD Received 19 Aug 2011; revised 3 Oct 2011; accepted 9 Oct 2011; published 2 Nov 2011

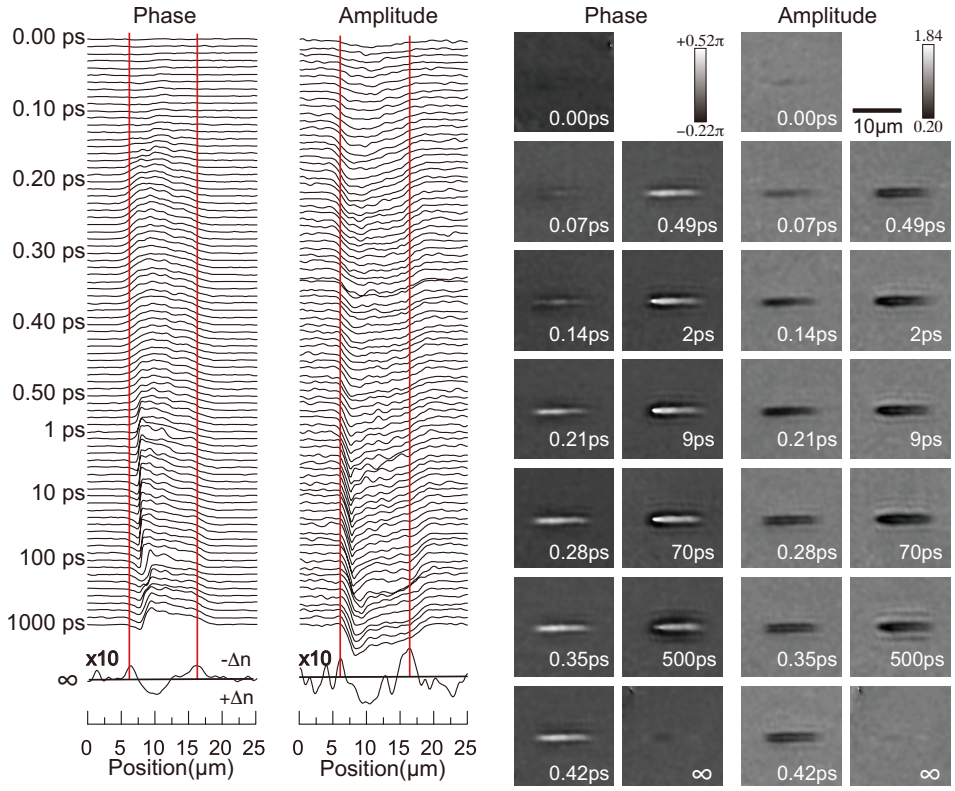

Fig. 2. Axial cross-sections and maps of the phase and amplitude at different time delays. Vertical lines are eyeguides of the focal region and are separated by 9 μm. Pulse energy $E_p = 200$ nJ. Intensity of the phase and amplitude images at $t \to \infty$ was $10^{\times}$ multiplied to make the changes recognizable. The amplitude image was divided by the reference image obtained before laser pulse irradiation and has the range between ~ 0.2 to 1.84. The pulse travels from left to right on the map images.

of void and densification. Pulse duration at the focus was optimized by pre-chirping in order to achieve the smallest energy of a recognizable modification. At such conditions the pulse duration is close to the spectral bandwidth-limited value of $\tau_p = 45 \pm 5$ fs in air. Once the chirp was optimized for the pump, part of the same pulse was used to generate probe strobing pulse. Its duration has not been measured but from the observed spatial resolution of the fastest phase and amplitude change side-view images can be estimated to be ~ 50 fs. Precision of the time delay in pump-probe measurements was $\Delta t = \pm 10$ fs determined by precision of the optical delay line.

3. Results and discussion

First, we present scenario of events which follow from phase images and are analyzed in details below. There are several distinct features discernable in time sequence of the phase images. Fast electronic excitation peaks toward the end of the pulse $\tau_p = 50$ fs, then the phase decrease due to recombination and diffusion ensues. Recombination delivers an efficient energy equilibration between electrons and ions/lattice in addition to the scattering. The fast nonlinear recombination

#153140 - $15.00 USD Received 19 Aug 2011; revised 3 Oct 2011; accepted 9 Oct 2011; published 2 Nov 2011

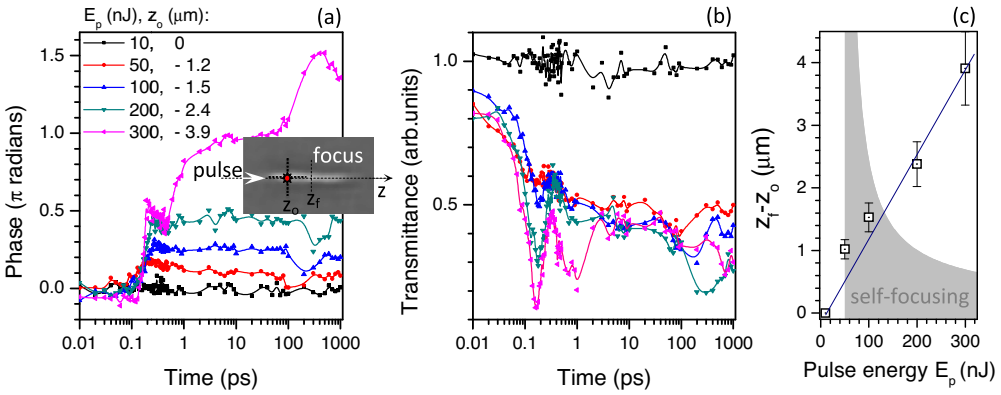

Fig. 3. Transients of the *on-axis* phase (a) and amplitude ((b) as in Fig. 2) at the observation point z_o, which is set at the location where the maximum phase change occurred during the entire observation time window; a negative shift on z-axis is measured from the center of the geometrical focus, z_f. The location z_o is where the void formation is expected and it is plotted in (c). Pulse energy E_p is estimated at the focal region. Gray region in (c) shows expected change of the self-focusing length according to scaling $z_{sf} \propto 1/(\sqrt{E_p/E_{cr}-1})$ [27] where self-focusing threshold was taken at power corresponding to the $E_{cr} = 50$ nJ or $P_{cr} \simeq 1$ MW/pulse.

(bimolecular and Auger) and the linear recombination (to a lower extent) triggers a build up of a thermo-elastic stress via volumetric expansion and lasts during 2-100 ps time span. Rarefied void-like structures are seeded after this time and release accumulated stress by formation of a free surface via cavitation. This launches pressure waves in the lateral direction; the lateral imaging is better suited to follow stress propagation due to a higher contrast as we demonstrated earlier [1]. On the longer time scale of 0.2 - 1 ns, there were axial movement and reshaping of the void-regions as imaged by movement and reshaping of the phase pattern. Finally, voids and a densified center is formed after the end of all relaxation processes.

3.1. Phase maps of the focal region during excitation and relaxation

Detailed sequence of phase map evolutions is given in Fig. 2. It shows cross sections of the axial transients and several selected phase maps. The length of the central filament is about 9 μm at its maximum and is longer about 4-5 times as the Rayleigh length at the used focusing. At the end of the all relaxation, $t \to \infty$, there is an observable densified central region at the location of geometrical focus and rarefied regions in front and behind it. The voids are formed at those regions at high pulse energies.

We set the point of observation of the phase changes at the point z_o where the largest phase changes occurred during the entire time of relaxation. This is an expected location of voids and it was always in front of the geometrical focus z_f due to self focusing. Figure 3(a) shows the phase changes followed in time at different pulse durations. The threshold of a detectable free electron plasma generation occurred at $E_p = 24$ nJ under the used focusing conditions [1]. At $E_p = 35$ nJ, a transient cavitation bubble was formed as observed in the lateral view [1]. The recognizable optical plasma emission - a spark - was observed at 50 nJ which is considered the dielectric breakdown threshold.

At the high laser pulse energy of $E_p = 300$ nJ the first phase jump occurs within $\sim$50 fs, which is close to the pulse duration $\tau_p = 45 \pm 5$ fs. This fast positive phase change, $\Delta\phi \simeq +0.6\pi$,

#153140 - $15.00 USD Received 19 Aug 2011; revised 3 Oct 2011; accepted 9 Oct 2011; published 2 Nov 2011

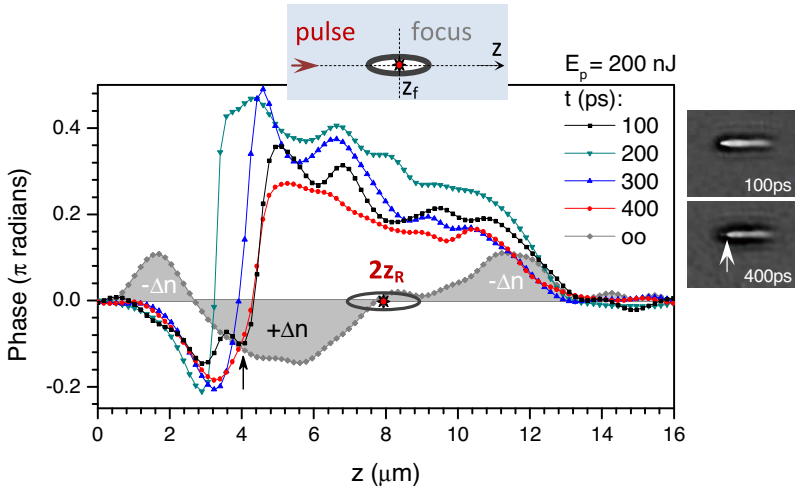

Fig. 4. The *on-axis* phase distribution close to the geometrical focus z_f, which is determined with ± 1 μm precision at different time moments. Pulse energy $E_p = 200$ nJ. Arrow shows the feature on the modification front which moved slower that speed of sound in solid glass.

is consistent with the ionization and a focus shift at the higher pulse energy is due to a stronger ionization rather than due to self focusing, which is limited at tight focusing; the critical power of self focusing is $P_{cr} \simeq 1$ MW or $E_p = 50$ nJ. The phase jump at smaller pulse energies was less steep corresponding to a different degree of ionization and the final electron concentration, n_e. After the fastest possible to resolve ionization when the maximum phase change $\Delta\phi \simeq +0.5\pi$ is achieved, there is a recognizable decay region lasting ~ 0.2 ps until a plateau is reached for the $E_p = 200$ nJ pulses. A new growing feature in the phase is observed for the $E_p = 300$ nJ pulse. The slope of this phase rise is $\gamma = 1$ (if plotted in a log-log presentation) signifying the linear mechanism and lasting for from ~ 0.6 to almost 100 ps. This time span corresponds well to the build up of the thermo-elastic stress after the electron-lattice energy equilibration finishes within $2-5$ ps. Since a lot of energy was deposited into the electronic sub-system, the equilibration together with recombination drives the phase even more positive due to heating. It is noteworthy, that the phase decay in the time window of $0.2-0.7$ ps is close to the $\propto \sqrt{t}$ indicating a diffusional character of the process. This could be a fast electron diffusion.

Figure 3(b) shows the amplitude maps at the same time windows as the phase (a). The fast amplitude change at the beginning of the pulse reflects absorption by free carriers followed by fast recombination (darker shade corresponds to the stronger absorption). The fast recombination causes heating and build up of thermal stress as discussed in the analysis of the phase maps. Since the absorption of glass is strongly dependent on its temperature and state (solid vs molten), the estimation of the absorption coefficient becomes complex and has not been carried out.

The clear rising feature after 100 ps in the case of $E_p = 300$ nJ is attributable to the void formation at the point of observation (note, it was set at the location of the largest phase change). The Fig. 3(c) shows that the location of the void was not affected by self focusing, whose expected scaling with pulse energy is plotted in gray scale. The length of the modified region was larger as the Rayleigh length, $2z_R$ at the employed focusing conditions, however, filamentation which is signature of self focusing [28] was not observed. This is consistent with absence of filamentation at tight focusing $NA > 0.9$.

#153140 - $15.00 USD Received 19 Aug 2011; revised 3 Oct 2011; accepted 9 Oct 2011; published 2 Nov 2011

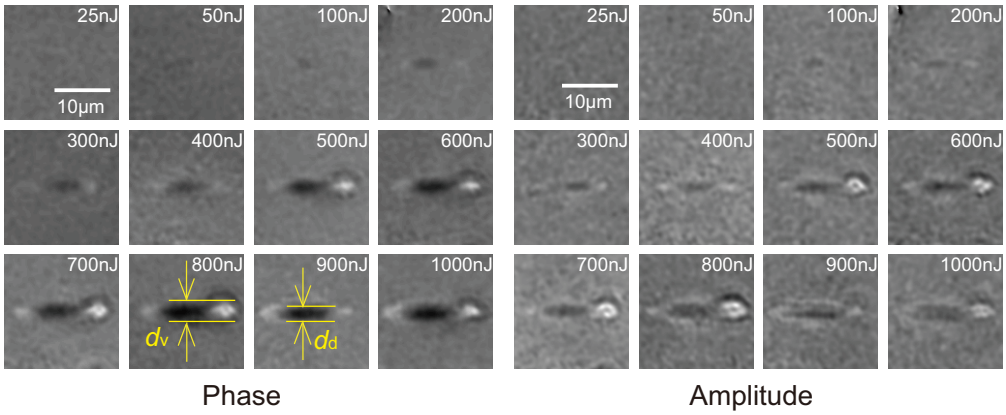

Fig. 5. Phase and amplitude maps after all relaxation processes $t \to \infty$ at several pulse energies; $d_{v,d}$ is the thickness of the void and denser phase, respectively, assuming cylindrical cross section.

3.2. *Estimations of plasma densities*

The initial electronic excitation part responsible for the phase change, $\Delta\phi$, (see the first step in Fig. 3) is directly related to the electron density via $\Delta\phi = \frac{\omega}{2cn_c}\int n_e dx = 2\pi D$, here $n_c = \varepsilon_0 m_e \omega^2/e^2 = 1.71\times10^{21}$ cm^{-3} is the critical electron density at $\lambda = 800$ nm wavelength, ε_0 is a permittivity of the free space, e, m_e is the electron charge and mass, respectively, $\omega = 2\pi c/\lambda$ is the cyclic light frequency, c is the speed of light in vacuum, and D is the ratio of the interference fringe shift in respect to the fringe period, Λ, i.e., for the shift equal Λ the corresponding phase is 2π and $D = 1$ [2]. The maximum free-carriers related jump of the phase was $\phi = 0.6\pi$ and would correspond to average electron density of $n_e = (4.1\pm0.3)\times10^{20}$ cm^{-3} assuming the width of the region $w = 2$ μm. This density is approximately 4 times lower than the critical density at 800 nm. The same phase change can be used to estimate the refractive index change Δn (negative) for the corresponding $\phi = \frac{\omega}{c}\int \Delta n dx$. One would find $\Delta n = -0.06$ for the effective thickness of the phase changed region $w = 2$ μm.

The phase changes after the fast electronic response are more complicated for interpretation since there are several contributions from the thermal expansion driven component, cavitation - the void formation, and movement of the void-like structures along the optical axis. Since the void would cause the largest possible contrast of refractive index $\Delta n = 0.5$ the diameter, d_v, of the void region for the phase change $\Delta\phi = +1\pi$ can be found from the phase delay, $\Delta\phi = \frac{2\pi}{\lambda}\Delta n d_v$; one would find $d_v = 0.4$ μm for imaging at $\lambda_{pr} = 400$ nm and is close to the expected size of voids generated in glasses [27].

Figure 4 shows the axial cross sections of the phase at different time moments. The axial phase maps reveal movement of the denser phase (a negative phase ϕ) along the propagation axis causing compression. Glass has a larger acoustic impedance at high temperature due to which the regions of positive phase change behaves as an acoustic waveguide. From the phase distributions on the optical axis at $t = 100$ and 400 ps (see, the front movement in Fig. 4), the estimated speed of the phase-change movement was $\sim 3.5\times10^3$ m/s (an arrow marking in Fig. 4), which is smaller than the sound speed of 5.4×10^3 m/s in glass at room conditions. As compression progresses in time (Fig. 4), a pressure back reflection develops which is simultaneous with an onset of a lateral movement of the denser phase towards the optical axis was observed at times >400 ps. This complex behavior cavitation, melt flow, compression, and solidification

#153140 - $15.00 USD Received 19 Aug 2011; revised 3 Oct 2011; accepted 9 Oct 2011; published 2 Nov 2011

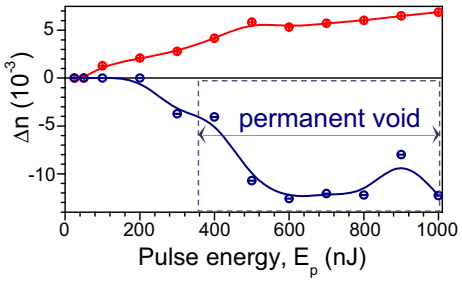

Fig. 6. Maximum refractive index changes, Δn calculated assuming the phase delay in a region of refractive index change of the thickness $d_{v,d}$ for the void and denser phase, respectively, according to $\Delta\phi = \frac{2\pi}{\lambda}\Delta n d_{v,d}$; the negative phase shift at $-\Delta n$ corresponds to the positive phase on the images (brighter regions). Region of energies when void is formed after all relaxation is shown in a box.

now can be seen at the limit of resolution of current setup and has to be further analyzed. It is driven by temperature, its gradient, surface tension, and phase liquid-solid transition [29]. The pressure converging onto and out from the optical axis can be seen on the phase and amplitude images. The wave closing onto the axis was responsible for the filling of the central cavity and formation of the denser phase after all relaxations. The two rarefied regions in front and at the end of the central denser regions are formed.

3.3. *Electron - ion relaxation time*

Estimation of the electron-lattice scattering time, τ_{e-i}, can be obtained using classical Drude model for the free electron absorption cross section determined by the dielectric function $\varepsilon = 1-\omega_p^2/[\omega(\omega+i\nu_{e-i})]$, here $\nu_{e-i} \equiv 1/\tau_{e-i}$, ω_p is the plasma cyclic frequency at critical plasma density n_c, and $i=\sqrt{-1}$. For this purpose we measured the relative intensities between the background and plasma regions: $I_b/I_{pl} = 1/0.14$, at the maximum absorption at $t = 0.16$ ps, for the $E_p = 300$ nJ. The corresponding value of τ_{e-i} directly follows from [2]:

$$\frac{\ln(I_b/I_{pl})}{4\pi n_0 D} \times \frac{1+\omega^2\tau_{e-i}^2}{\omega\tau_{e-i}} = 1, \tag{2}$$

and one would find $\tau_{e-i} \simeq 1.1$ fs for the $D \equiv \Delta\phi/2\pi = 0.6$ which is the largest phase modification at the end of laser pulse (Fig. 3) with approximate electron density $n_e \sim 10^{20}$ cm^{-3}. In silica, $\tau_{e-i} \simeq 2$ fs [2, 27] and it is weakly dependent on the electron density. In the critical plasma - under optical breakdown - it is usually assumed that the $\tau_{e-i} \simeq 0.9$ fs or in terms of frequency $1/\tau_{e-i} \simeq 10^{15}$ s^{-1} [27]. The obtained value of $\tau_{e-i} = 1.1$ fs is consistent with typical values observed in different glasses [2, 27] and it is shorter than the optical period of 2.67 fs at 800 nm wavelength.

3.4. *End of relaxation*

Figure 5 summarizes the final refractive index modifications after all stages of relaxation end. The center of an on-axis region has an augmented refractive index, $+\Delta n$, and optically less dense regions are formed in front and behind of it along the pulse propagation. For the pulses energies exceeding approximately 300 nJ there is a distinct void presence. The voids were observed before at a comparable tight focusing, however, at smaller pulse energies/irradiance in sapphire and high purity silica [27, 30, 31]. The main difference from current experiments

#153140 - $15.00 USD Received 19 Aug 2011; revised 3 Oct 2011; accepted 9 Oct 2011; published 2 Nov 2011

in glass is the presence of a weak self-focusing and axial smearing of the pulse energy as can be seen from Fig. 2. Also, sapphire and silica have a high temperature of melt-solid transition which helped to freeze laser induced modifications more efficiently. This tendency was further revealed in more details in ref. [32].

Crown glass has a considerable concentration of glass modifiers as opposed to the pure Si- and B-oxides which are the glass formers [32] with bond energies 4.60 and 3.86 eV, respectively. There is a strong melt reflow to the central part where initially the void is formed after typically 100 ps (see, Fig. 3). As re-solidification progresses a less viscous (higher temperature) melt is pushed out from the regions were solidifications starts (the regions located further away from the center). This finally results in formation of the lower density, rarefied and void regions upon solidification. Presence of self focusing did not distort modified volume beyond central region of $\sim 10\ \mu$m. The length and width of the denser phase, Δn, scales almost linearly with the pulse energy, E_p, between 100 and 1000 nJ (Fig. 6). This is a welcome feature for the waveguide writing using tightly focused laser pulses. It is noteworthy, that during a stage of a molten phase and a presence of a free void surface, there is a possibility of strong restructuring via surface tension gradients [33] and can be beneficial for the glass doping via preferential incorporation of glass modifiers into the re-solidified irradiated region. This opens new strategies to prepare glass composition for self-doping or self-densification as discussed recently [15].

4. Conclusions

We have demonstrated interferometric side-view imaging of glass modification by single short (~ 50 fs) fs-laser pulses with the highest spatial and temporal resolution to date. The breakdown, electronic and thermo-elastic modifications of the focal region in glass were tracked in time revealing detailed mechanisms and evolution of the structural modifications leading towards central void formation and melt reflow and freezing-in the final voids and densified regions adjacently along the pulse propagation. Densified glass regions can be used for waveguide formation which can be in situ monitored with high spatial and temporal resolution.

Using Drude approximation we measured the electron-ion relaxation time $\tau_{e-i} \simeq 1.1$ fs at strong excitation in glass. Further improvements of axial resolution by optical imaging are technically difficult due to geometrical constrains of two objective lenses working at 90° angle to each other and at a short $\sim 100\ \mu$m working distance. The side-view imaging of fs-laser pulse induced phenomena from void formation to densification could be achieved with synchronized ultra-short X-ray pulses and would provide a necessary advancement in spatial and temporal resolution. Time-space characterization of the 3D laser structuring in different materials is key towards development of new materials, optimized exposure conditions [34–39], and revealing the fundamental mechanisms of light-matter interaction [40–46].

Acknowledgments

This work was supported by a Grant-in-Aid for Scientific Research (B) from the Ministry of Education, Culture, Sports, Science and Technology of Japan.

#153140 - $15.00 USD Received 19 Aug 2011; revised 3 Oct 2011; accepted 9 Oct 2011; published 2 Nov 2011